ELSEVIER

Journal of Quantitative Spectroscopy & Radiative Transfer 88 (2004) 267–284

Journal of Quantitative Spectroscopy & Radiative Transfer

www.elsevier.com/locate/jqsrt

The negative polarization of light scattered from particulate surfaces and of independently scattering particles

Yu. Shkuratov[a,*], A. Ovcharenko[a], E. Zubko[a], H. Volten[b,c], O. Muñoz[d], G. Videen[e]

[a]*Astronomical Institute, Kharkov National University, 35 Sumskaya St. Kharkov. 61022, Ukraine*
[b]*Astronomical Institute "Anton Pannekoek", University of Amsterdam, Kruislaan 403, NL-1098 SJ, Amsterdam*
[c]*FOM-institute AMOLF, Kruislaan 407, NL-1098 SJ, Amsterdam, Netherlands*
[d]*Instituto de Astrofísica de Andalucía, CSIC, Camino Bajo de Huétor 24, Granada 18008, Spain*
[e]*Army Research Laboratory AMSRL-CI-EM, 2800 Powder Mill Road, Adelphi, Maryland 20783, USA*

Received 24 February 2004; accepted 25 March 2004

Abstract

Laboratory and computer modeling investigations of the negative polarization of particulate surfaces at small phase angles are important in the development of remote-sensing research of atmosphereless celestial bodies. We present measurements of the phase-angle dependence of the intensity and degree of linear polarization of particles in air and particulate surfaces composed of the particles at illuminating wavelengths 0.63 and 0.44 μm. The particulate surface measurements were carried out with the equipment at the Kharkov National University; whereas the scattering measurements of single particles were carried out with the Amsterdam equipment. We study a suite of samples of natural mineral particles (including two volcanic ash samples) that are characterized by a variety of shapes and colors. We find evidence that suggests that in some instances the negative polarization of the surfaces is a remnant of the negative polarization of the single scattering by particles constituting the surfaces. Computer simulations of the light scattering from the particulate surfaces support this conclusion.
Published by Elsevier Ltd.

Keywords: Negative polarization; Opposition effect; Ray-tracing; Coherent backscattering

1. Introduction

Planetary regoliths demonstrate the brightness opposition spike and accompanying negative polarization at small phase angles [1]. The latter was discovered by Lyot [2] in 1929 during lunar observations

* Corresponding author. Tel.: +38-057-702-2207; fax: +38-057-243-2428
E-mail address: shkuratov@vk.kh.ua (Yu. Shkuratov)

0022-4073/$ - see front matter Published by Elsevier Ltd.
doi:10.1016/j.jqsrt.2004.03.029

and was also observed in many terrestrial particulate surfaces. The interpretation of decades of polarimetric data obtained from telescopic observations and laboratory measurements was not satisfactory until the coherent backscattering mechanism was suggested as the explanation of both the brightness and polarimetric opposition phenomena [3–22]. Recently much additional experimental data were obtained showing that the effects are more complex than previously considered [23,24]. In particular, negative polarizations with double-minima were found for satellites of Jupiter and bright asteroids [25,26]. These observations suggest that there may be two different branches, a narrow, asymmetric branch sometimes referred to as the polarization opposition effect (POE) and a wider, symmetric branch sometimes referred to as the negative polarization branch (NPB). These two branches may have different mechanisms: the narrow POE appears to be dominated by coherent backscattering, the constructive interference of reciprocal rays; whereas, there is still some debate as to the mechanism for the NPB. In this manuscript we focus on the NPB. In laboratory investigations the NPBs of particulate surfaces reveal very different characteristics; in particular, the shape of NPBs varies depending on choice of material, characteristics of particles, and packing density of the surfaces [23,24].

In principle, the NPB of a regolith-like surface can be formed by two mechanisms: the coherent multiple scattering as well as the single scattering by particles (e.g., [23]). The role of single scattering in the formation of the opposition phenomena was first discussed by Hapke [27]. It is not clear yet which mechanism dominates. Here we attempt to link experimentally the NPBs produced by scattering from an ensemble of well separated polydisperse particles in air and particulate surfaces composed of the same particles. To compare scattering properties of particulate surfaces with those of individual particles we use laboratory measurements and computer modeling. We study samples of different mineral composition [28–33]. For computer experiments we use the discrete-dipole approximation (DDA) method in the version presented in [34–37]. The method is exploited to calculate single scattering by irregular particles. For calculations of light scattering by particulate surfaces (media) we use the Monte-Carlo ray-tracing technique [23,38].

2. Instruments and samples

For this work we use two laboratory instruments: (1) the Kharkov photometer/polarimeter and (2) the Amsterdam nephelometer. The first instrument allows measurements of the intensity and degree of linear polarization of light scattered from powdered surfaces when the incident light is unpolarized; the second one is used to determine all 16 elements of the Mueller matrices of ensembles of independently scattering particles in air. We briefly describe the instruments below.

2.1. Kharkov setup

The small-phase-angle photometer/polarimeter is used to study phase curves of reflectance and degree of linear polarization of scattered light, providing measurements for surfaces with complicated structure including powders in the phase angle range of 0.2°–17° [23,39–41]. It employs halogen lamps as unpolarized light sources. For this study, we select wide spectral bands centered at $\lambda_{red} = 0.63$ μm and $\lambda_{blue} = 0.45$ μm. All measurements are carried out at the illumination/observation geometry when samples are viewed with the detector along the sample normal. The rotated light source arm changes the incidence angle that is the phase angle α. The definition of the sample albedo A used in this paper is the

reflectance of the sample surface measured at $\alpha = 2^\circ$ relatively to a compressed Halon sample that we use as a reflectance standard (a "Lambertian" screen) for comparison at the same phase angle and wavelength with other samples. We note the small-phase-angle-range photometer/polarimeter was calibrated against a comparable JPL NASA instrument [42].

The average accuracy of our measurements is within 0.05%, including random and systematic errors. The accuracy is somewhat less when extremely dark surfaces, like carbon soot, are measured. Measurements are repeated at different times to test for reproducibility. Typically, differences are within 0.05%.

2.2. Amsterdam instrument

A portion of the measurements presented in this paper for comparison was obtained with the Amsterdam instrument and has been published previously [28–32]. A detailed description of the instrument that was used to measure the scattering matrices of ensembles of independently scattering particles is given in [33,53]. In this work, only two of the matrix elements are used: $F_{11}(\alpha)$ and $F_{12}(\alpha)$. We briefly explain how the measurements were carried out. A HeNe laser (633 nm, 5 mW) or a HeCd laser (442 nm, 40 mW) is used as a light source. Thus, the wavelengths are close to those used in the Kharkov instrument. The laser light is modulated with an electro-optic modulator. The modulated light is subsequently scattered by the ensembles of randomly oriented particles located in a jet stream produced by an aerosol generator. The configuration of the optical components allows for the simultaneous measurements of the scattering function $F_{11}(\alpha)$ and the ratios $-F_{12}(\alpha)/F_{11}(\alpha)$. The scattered light is detected with a photomultiplier that moves along a circular ring, in the center of which the particle stream is located. A range in phase angles α is covered from 175° (nearly forward scattering) to 7° (nearly backward scattering).

The values obtained for the measured Mueller matrix elements are the average of several data points, and the corresponding experimental error is the standard deviation of the mean value [33]. The experimental setup was tested by comparing results of water-droplet measurements to results of Lorenz–Mie calculations for homogeneous spherical particles finding an excellent agreement over the entire angle range for all scattering matrix elements [33].

2.3. Samples

We measured scattering matrices for a wide variety of natural mineral samples including two volcanic ash samples. The projected surface-area distributions have been measured using a Fritsch laser particle sizer [43]. In Table 1 we present a brief characterization of each sample including the effective radius r_{eff} and effective variance v_{eff} as defined by Hansen and Travis [44]. In Table 1 we also give the most abundant mineral constituents and colors of the samples. Most of our natural samples present a wide variety of irregular shapes. For instance, the fly ash aerosol particles, whose total dimensions are characterized by r_{eff} and v_{eff}, consist of aggregates of nearly spherical particles. More detailed information about the materials can be found in [28–33] including scanning electronic microscope pictures of particles and their size distributions (see also http://www.astro.uva.nl/scatter/).

The surface of samples measured with the Kharkov instrument was formed with free fall of powders on the bottom of a sample cup without packing and smoothing the surface. We insert in Figs. 1–10 photomicrographs of the particulate surfaces. The images were obtained with an optical microscope; the dimensions of all the images are 1 mm × 1 mm.

Table 1
Data on samples studied

Sample	Main constituents	r_{eff} (μm).	v_{eff}	Color	
Feldspar	K-feldspar, plagioclase, quartz	1.0	1.0	Light pink	
Green clay	Illite, kaolinite, montmorillonite, quartz	1.55	1.4	Green	
Red clay	Biotite, illite, quartz	1.5	1.6	Red	
Loess	K-feldspar, illite, quartz, calcite, chlorite, albite	3.9	2.6	Yellow brown	
Lokon volcanic ash	Silica glass, plagiocalse, magnetite	7.1	2.6	Dark brown	
Pinatubo volcanic ash	Silica glass, plagioclase, amphibole, magnetite	3.0	12.3	Light gray	
Olivine L	Mg-rich olivine				
	($Mg_{1.8}Fe_{0.14}SiO_4$)	3.8	3.7	White	
Olivine M	Mg-rich olivine				
	($Mg_{1.8}Fe_{0.14}SiO_4$)	2.6	5.0	White	
Olivine S	Mg-rich olivine				
	($Mg_{1.8}Fe_{0.14}SiO_4$)	1.3	1.8	White	
Fly ash	Clay minerals	3.65	10.9	Gray brown	

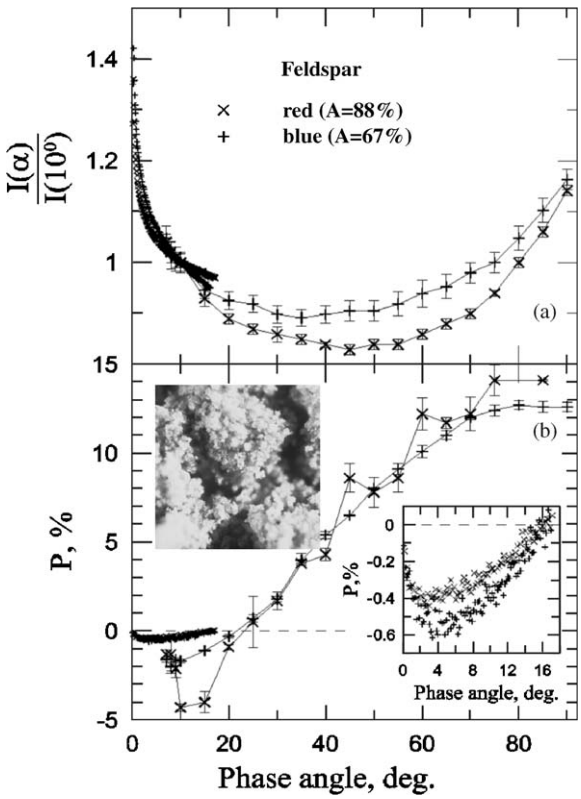

Fig. 1. Phase curves of normalized intensity (a) and degree of linear polarization (b) for samples of feldspar in red and blue light. Large symbols correspond to single scattering measurements. Small symbols present particulate surface data. The inserted plot placed in the bottom right corner is a magnified portion of polarimetric data for the particulate surface. Another inset is a microscopic image of the particulate surface. The albedo values correspond to measurements of the particulate surface.

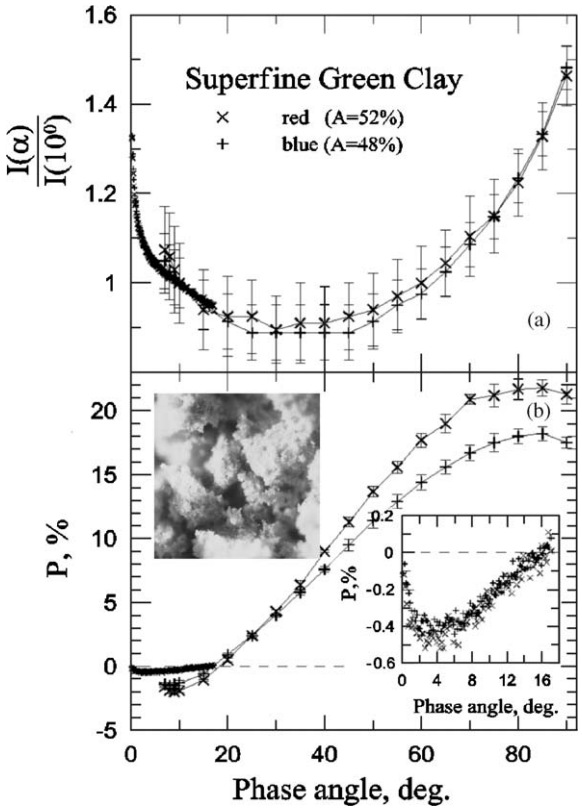

Fig. 2. Phase curves of normalized intensity (a) and degree of linear polarization (b) for samples of superfine green clay in red and blue light. Large symbols correspond to single scattering measurements. Small symbols present particulate surface data. The inserted plot placed in the bottom right corner is a magnified portion of polarimetric data for the particulate surface. Another inset is a microscopic image of the particulate surface. The albedo values correspond to measurements of the particulate surface.

3. Experimental results

Results of our photometric and polarimetric measurements are given in Figs. 1–10. The scattering intensities for particles in air and particulate surfaces are normalized to 1 at $\alpha = 10°$. The experimental errors for the single-scattering measurements are indicated with bars. When no error bar is shown, the value for the standard deviation of the mean value is smaller than the symbol plotted. Magnified plots for polarimetric phase curves corresponding to particulate surfaces are presented in the insets. The measurement errors of particulate surfaces can be estimated from the point dispersion on the plots; the errors are fairly small.

As shown in Figs. 1–10, all the single scattering phase functions, $F_{11}(\alpha)$, follow the general trends presented by irregularly shaped mineral particles [28–33]. Most of the light is scattered toward large phase angles and there tends to be a modest rise at small phase angles. This rise is more pronounced for the fly ash particles that consist of aggregates of spheres. The particulate surfaces show steep peaks at very small phase angles, where we do not have measurements for particles in air. Comparisons of

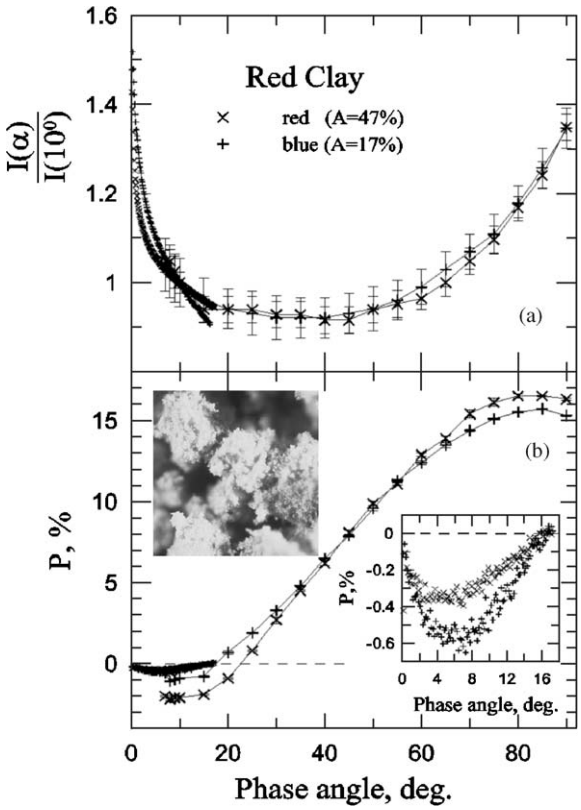

Fig. 3. Phase curves of normalized intensity (a) and degree of linear polarization (b) for samples of red clay in red and blue light. Large symbols correspond to single scattering measurements. Small symbols present particulate surface data. The inserted plot placed in the bottom right corner is a magnified portion of polarimetric data for the particulate surface. Another inset is a microscopic image of the particulate surface. The albedo values correspond to measurements of the particulate surface.

the brightness phase functions for particles in air and particulate surfaces suggest that the opposition brightness surges of the surfaces might be formed partially with the contribution of single scattering at phase angles 7°–20°. It should be remembered that incoherent multiple scattering partially suppresses this contribution and therefore, slopes of phase functions of particulate surfaces are lower at the phase angle range than in the case of particles in air. Brightness spikes of particulate surfaces seen at phase angles less than 7° are caused by the coherent backscatter enhancement and shadow-hiding effect.

All measurements for particles in air presented in this work show NPBs at positions close to the backward direction with $|P_{\min}|$ up to 5%. These NPBs are produced under single scattering conditions. This allows us to hypothesize that the single scattering NPBs could be the dominant factor in the NPBs of the surfaces consisting of the particles. In this case the NPBs that are seen on the insert plots of Figs. 1–10 may be treated as remnants of the NPBs of the single scattering. The NPB amplification for particulate surfaces with decrease in albedo can be considered as evidence for this hypothesis, since incoherent multiple scattering increases as albedo increases and suppresses features of single scattering, like the NPBs. Indeed, Figs. 1 and 2 show that the single scattering NPB of green clay (darker sample) is almost

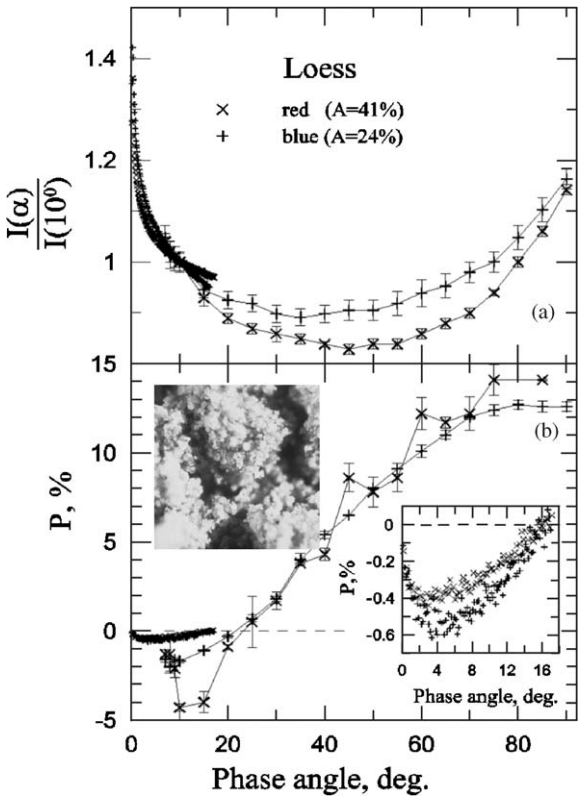

Fig. 4. Phase curves of normalized intensity (a) and degree of linear polarization (b) for samples of loess in red and blue light. Large symbols correspond to single scattering measurements. Small symbols present particulate surface data. The inserted plot placed in the bottom right corner is a magnified portion of polarimetric data for the particulate surface. Another inset is a microscopic image of the particulate surface. The albedo values correspond to measurements of the particulate surface.

two times less than that of feldspar (brighter sample). Nevertheless the particulate surface NPBs of both these materials are almost the same, because the single scattering NPB of feldspar is suppressed due to high albedo of feldspar material. This is also seen for the Lokon and Pinatubo volcanic ash measurements (see Figs. 5 and 6). The single-scattering NPB of Lokon (smaller albedo) is smaller than the measurements for Pinatubo volcanic ash that shows a higher albedo. Again, the particulate surface NPBs of both volcanic ashes are virtually the same.

This result is consistent with measurements of the colored samples of red clay and loess (see Figs. 3 and 4). In fact the values of $|P_{\min}|$ of loess and red clay particles in red light are noticeably higher than in blue light.In contrast for particulate surfaces, the value $|P_{\min}|$ is higher in blue light as albedo of the powders in blue light are three times less than in red light.Therefore it seems like an increase of incoherent multiple scattering effects (when increasing albedo) produces a decrease of powder $|P_{\min}|$.Additional evidence that the NPBs of particles in air and of particulate surfaces have a common cause is the transformation of the NPBs for olivine samples presented with particles of different sizes (cf.Figs. 7–9).The

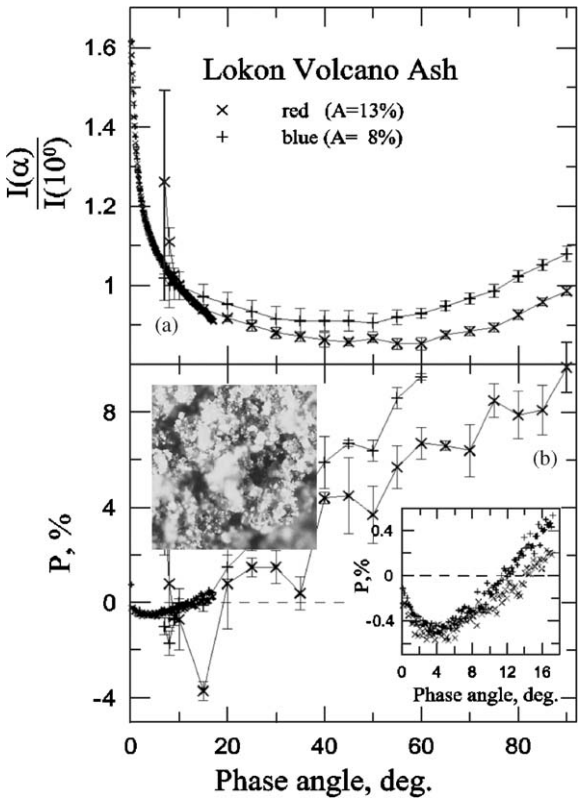

Fig. 5. Phase curves of normalized intensity (a) and degree of linear polarization (b) for samples of Lokon volcano ash in red and blue light. Large symbols correspond to single scattering measurements. Small symbols present particulate surface data. The inserted plot placed in the bottom right corner is a magnified portion of polarimetric data for the particulate surface. Another inset is a microscopic image of the particulate surface. The albedo values correspond to measurements of the particulate surface.

olivine samples were obtained from the same original rock.Therefore, the primary physical differences between these three samples are related to the size of their particles.Olivine L presents the largest r_{eff} and olivine S corresponds to the smallest r_{eff} (see Table 1).Figs. 7–9 demonstrate that the smaller the particle size, the stronger the NPBs of particles in air and particulate surfaces; i.e.the inversion angle and $|P_{\min}|$ of the particle NPBs correlate with those of surfaces.Other evidence that the NPBs of particles in air and of particulate surfaces may have a common origin is presented in Fig. 10 that shows measurements for the fly ash.This sample consists of small spherical particles forming aggregates, and shows strong backscattering and a remnant of the first rainbow.The rainbow feature (positive "surge" at $\alpha \approx 10°$) is seen clearly on the polarimetric phase curve corresponding to the particulate surface, although with some amplitude decrease that is caused by the incoherent multiple scattering between particles.Note that the feature is too weak to be seen on the photometric phase curves.The measurements of the fly ash are entirely consistent with our earlier measurements of particulate surfaces composed of glass spheres with sizes of 50–100 μm [23,41].

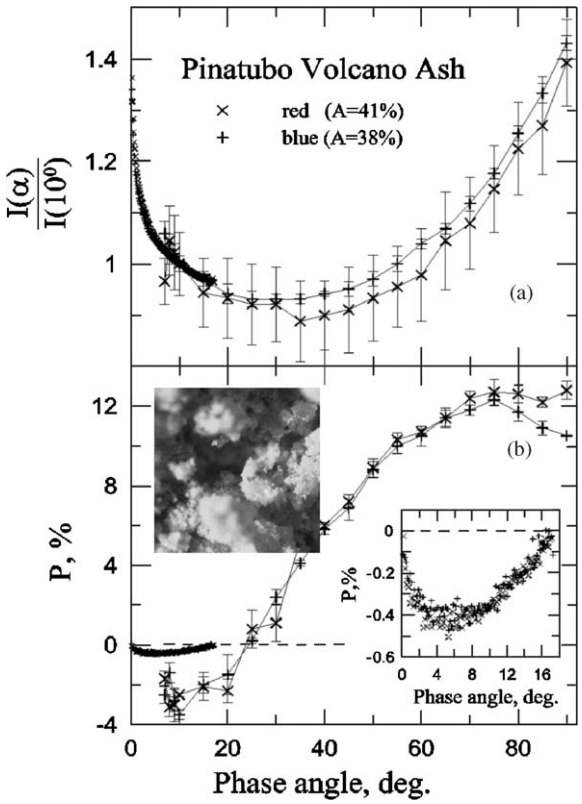

Fig. 6. Phase curves of normalized intensity (a) and degree of linear polarization (b) for samples of Pinatubo volcano ash in red and blue light. Large symbols correspond to single scattering measurements. Small symbols present particulate surface data. The inserted plot placed in the bottom right corner is a magnified portion of polarimetric data for the particulate surface. Another inset is a microscopic image of the particulate surface. The albedo values correspond to measurements of the particulate surface.

4. Computer simulation and discussion

To better understand the contributions of single scattering, coherent backscattering, and shadow-hiding, we carried out a computer simulation of scattering of particulate surfaces (media) composed of irregular and nearly spherical particles. To calculate the scattered light we used a combination of DDA and ray-tracing techniques. To estimate the coherent backscattering and shadow-hiding effects we applied the ray-tracing method using an average single-particle indicatrix calculated with the DDA.

The DDA method is described in many works, e.g., [45–50]. Thus we present here only the model of the irregular particles exploited here. To simulate them, a set of 137 376 cells is used to form an approximately spherical volume. Then a number of randomly chosen cells of the volume are marked as seeds of the particle material and empty space. Each cell that differs from the seeds is marked as the nearest seed cell. Examples of irregular particles used in our calculations are shown in Fig. 11. We also used spherical particles approximated by the lattice of dipoles (nearly spherical particles).

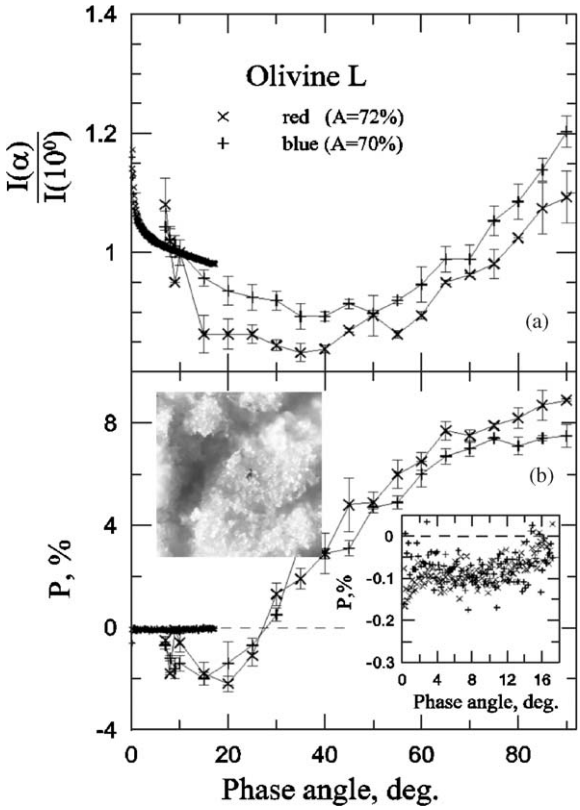

Fig. 7. Phase curves of normalized intensity (a) and degree of linear polarization (b) for samples of olivine L in red and blue light. Large symbols correspond to single scattering measurements. Small symbols present particulate surface data. The inserted plot placed in the bottom right corner is a magnified portion of polarimetric data for the particulate surface. Another inset is a microscopic image of the particulate surface. The albedo values correspond to measurements of the particulate surface.

We then apply a Monte Carlo ray-tracing technique to calculate the coherent backscattering effects [23,38,51] in particulate media. To generate a random medium with a given volume density ρ, we use a cubic box consisting of scatterers of a finite size. The upper side of the box corresponds to the boundary of the medium; the boundary is flat on average. The other sides of the box are cyclically conjugated (e.g., if a ray goes out of the box through the bottom, it returns into the box through the top). Since our calculations are time consuming, we have restricted them to six orders of scattering, which is sufficient for dark media [23]. Typically the initial cubic box contains 5000 particles and the number of rays is 1000. We usually use 10 000 different samples of the medium for averaging.

The model underwent different tests. In one such a test, we compare it with laboratory measurements of dark particulate surfaces. For instance, Fig. 12 shows results of our computer simulation and laboratory measurements with the Kharkov instrument of smoked carbon soot with albedo of about 2%: DDA-calculated scattering from model particles presented in Fig. 11 (curve 1) is used to generate the polarization response of a powder composed of such particles using the ray-tracing method (curve 2). The carbon soot substrate is a very fluffy dark surface with a low volume density. An asymmetric polarization response

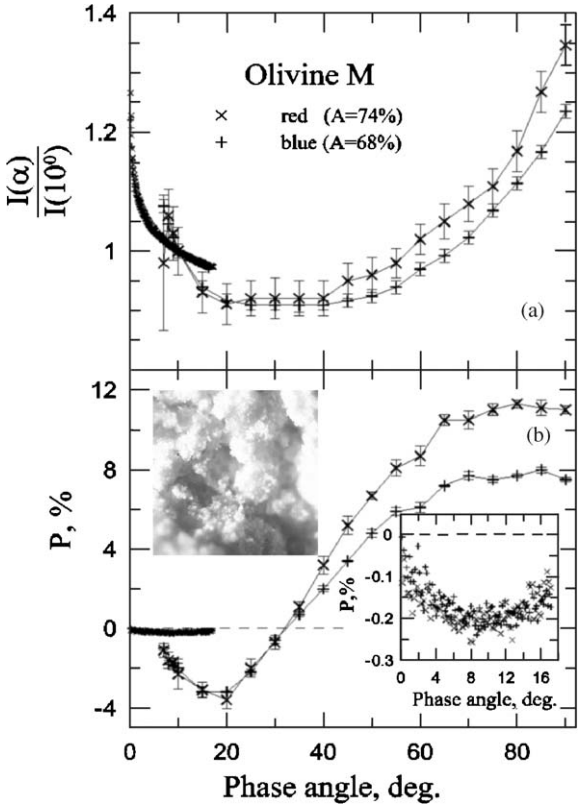

Fig. 8. Phase curves of normalized intensity (a) and degree of linear polarization (b) for samples of olivine M in red and blue light. Large symbols correspond to single scattering measurements. Small symbols present particulate surface data. The inserted plot placed in the bottom right corner is a magnified portion of polarimetric data for the particulate surface. Another inset is a microscopic image of the particulate surface. The albedo values correspond to measurements of the particulate surface.

is observed in this case. To model the measurements of carbon soot, we made calculations for particles with the size parameter of the equivalent sphere $x_{eq} = 2$ ($x_{eq} = 2\pi r/\lambda$, where λ is the wavelength and r is the sphere radius) and refractive index $m = 1.5 + 0.1i$, setting $\rho = 0.07$. The latter seems to be reasonable for the fluffy carbon soot surface [23]. As seen in Fig. 12, rather good coincidence is observed for the results of laboratory and computer experiments.

We next use the model to study the effect of multiple scattering in particulate media on single-particle NPBs. We first consider the case when the single particles do not display a NPB shown in Curve 1 of Fig. 13 for nearly spherical particles of $x = 1$ and $m = 1.5 + 0.05i$. When these particles compose a particulate surface with $\rho = 0.3$, a NPB may be formed (Curve 2) due to constructive interference of reciprocal rays traveling between particles.

Curve 3 in Fig. 13 shows the backscatter polarization from nearly spherical particles that display a strong NPB ($x = 5$ and $m = 1.5 + 0.5i$). When these particles compose a particulate surface ($\rho = 0.3$), the multiple scattering between particles noticeably weakens the NPB. Nevertheless, the asymmetry of the single-particle scattering NPB is clearly revealed in the case of the surface. Note that the asymmetric

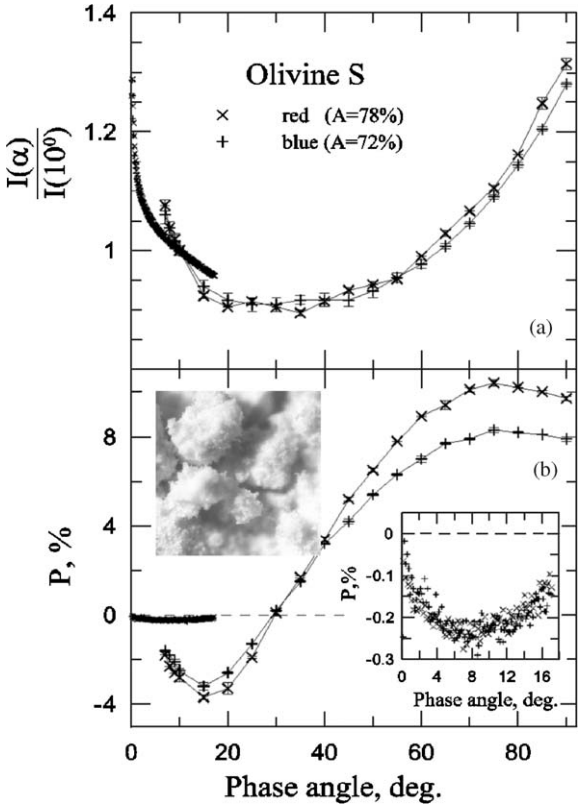

Fig. 9. Phase curves of normalized intensity (a) and degree of linear polarization (b) for samples of olivine S in red and blue light. Large symbols correspond to single scattering measurements. Small symbols present particulate surface data. The inserted plot placed in the bottom right corner is a magnified portion of polarimetric data for the particulate surface. Another inset is a microscopic image of the particulate surface. The albedo values correspond to measurements of the particulate surface.

minimum in both the single-scattering and multiple scattering systems of Fig. 13 is located toward larger phase angles. In the case of multiple scattering the asymmetry depends on ρ (cf. Figs. 12 and 13).

Thus our calculations show that the multiple scattering in the particulate surfaces weakens the NPB generated by single-particle scattering and has little influence on the shape of this NPB at $\rho = 0.3$. This deduction is in agreement with our measurements. In Figs. 2 and 3, the amplitude of the minimum of the degree of linear polarization for particulate surface is attenuated when compared with measured results for particles in air. The position of the minimum in both cases presents slight differences. In Fig. 10, a relative maximum of the degree of linear polarization for particles in air is located around 10°. This maximum is lower in the case of particulate surface, though is located at the same position.

Comparison of the curve pairs 1, 2 and 3, 4 in Fig. 13 shows that coherent multiple scattering between particles can generate the NPB when single particles do not have a NPB, but also may decrease the NPB if the single particles do have a NPB. We emphasize once again that the multiple scattering in particulate surfaces shifts the angle of polarization minimum of single-particle scattering toward smaller phase angles

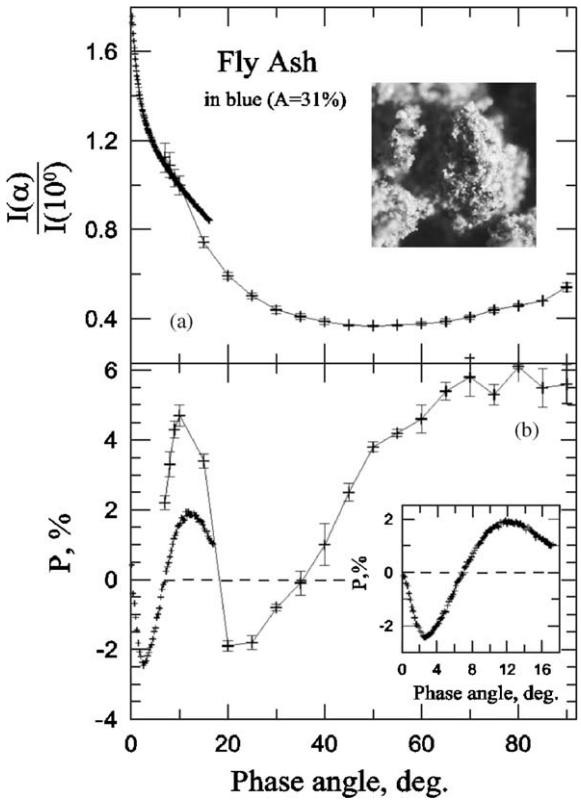

Fig. 10. Phase curves of normalized intensity (a) and degree of linear polarization (b) for samples of fly ash in blue light. Large symbols correspond to single scattering measurements. Small symbols present particulate surface data. The inserted plot placed in the bottom right corner is a magnified portion of polarimetric data for the particulate surface. Another inset is a microscopic image of the particulate surface. The albedo values correspond to measurements of the particulate surface.

(compare minima of curves 3 and 4 of Fig. 13) depending on the value of ρ. This effect is observed in laboratory experiments (cf. Figs. 1–9).

In the simulations of Fig. 14, we use the experimentally measured scattering characteristics of particles in air as the scattering indicatrix for Monte-Carlo simulations. We use the experimental phase-angle curves for intensity and polarization degree of the Lokon volcanic ash shown in Fig. 5, because the albedo of the sample is relatively low. This allows us to limit calculations to 6 orders of scattering. In our simulation, we take $\rho = 0.1$ and $x = 90$ that is close to the real data at blue light. Curve 1 in Fig. 14 presents experimental data for the aerosolized volcanic ash (see Fig. 5). The curve was obtained using a parabolic approximation of the data at the condition that the polarization degree equals zero at $\alpha = 0$. Note that the Monte-Carlo simulation employs the entire angle-dependent phase function. Curve 2 corresponds to our simulation of light scattering by a particulate surface composed of such particles. The open circles are the result of measurements of a particulate surface formed with the Lokon volcanic ash. The albedo of the particulate surface is about 6%. The calculated curve 2 exhibits the double-minima (bi-modal) structure that has been observed and discussed previously [25,26,52]. The minimum at smaller phase

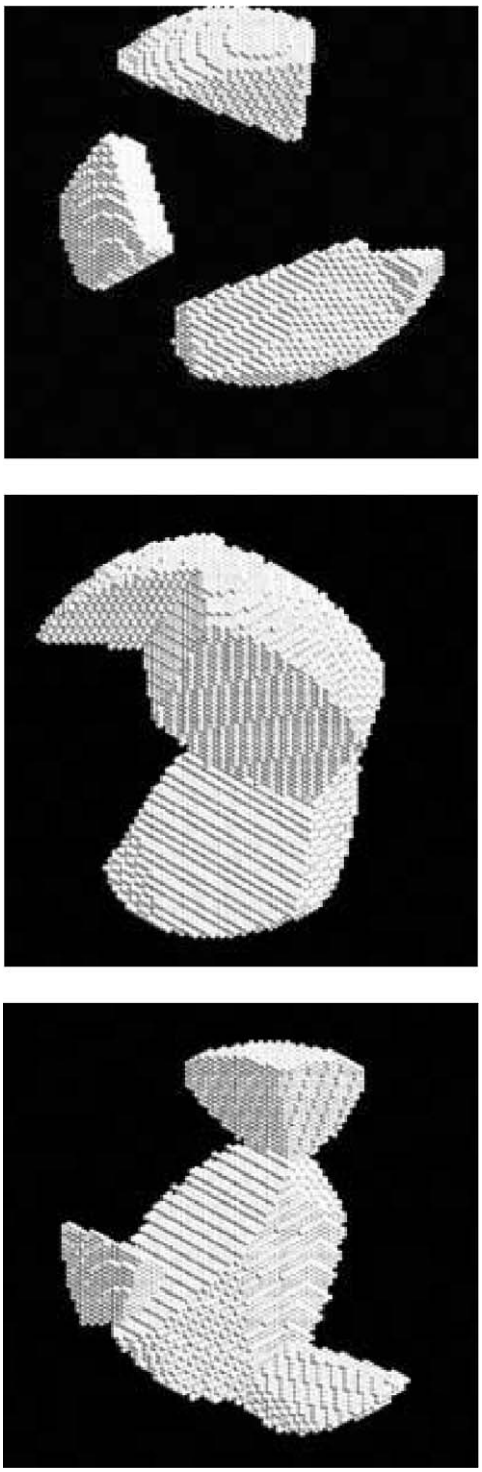

Fig. 11. Models of particles used for DDA and then ray-tracing calculations.

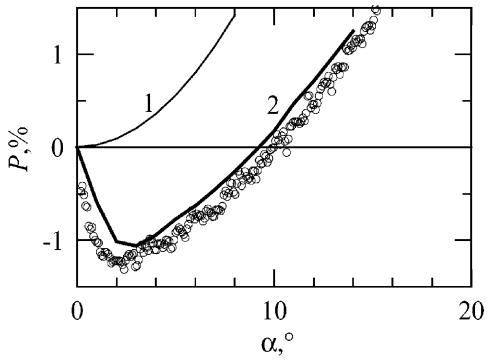

Fig. 12. DDA-calculated scatter from model particles of Fig. 11 (curve 1) is used to generate the polarization response of a substrate composed of such particles ($\rho = 0.07$) using ray-tracing (curve 2). Points correspond to Kharkov laboratory measurements of carbon soot.

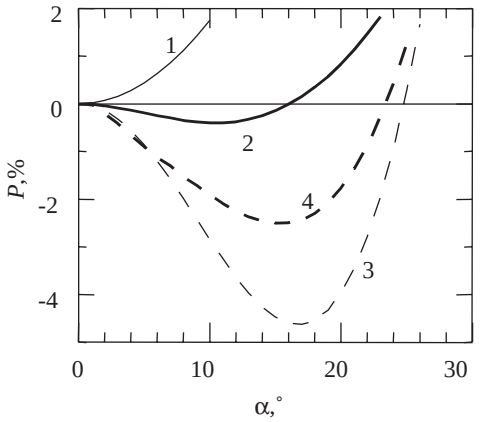

Fig. 13. Computer simulation of the NPBs when Curve 1: spherical particles in air that do not have a NPB ($x=1$ and $m=1.5+0.05$i); Curve 2: these particles compose a surface ($\rho=0.3$); Curve 3: spherical particles in air that have a NPB ($x=5$ and $m=1.5+0.5$i); and Curve 4: these particles compose a surface ($\rho = 0.3$).

angles is due to the coherent backscattering mechanism acting between individual particles. Comparison of the theoretical and experimental curves for the powder shows a resemblance at the larger phase angles. This suggests that the NPB mechanism of the particulate surfaces is the single-particle scattering NPB. It should be noted however that some discrepancies do occur, and the measurements do not reveal the narrow, large-amplitude POE spike that is predicted with the model, although some hint of a narrow spike exists in the experimental data. These differences may be the result of a shift of the spike to small phase angles that cannot be observed with the Kharkov apparatus.

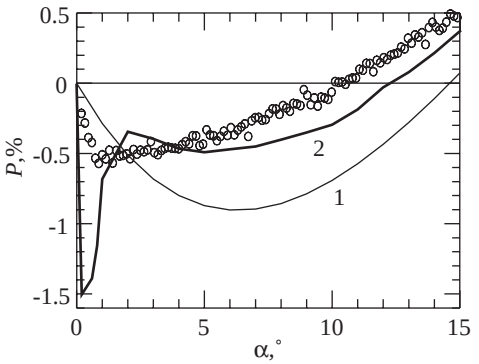

Fig. 14. Measured (symbols) and calculated (curve 2) polarimetric data for a surface composed of the Lokon volcanic ash. Curve 1 corresponds to the parabolic fit of backscattered portion of Fig. 5 for particles in air at the wavelength 440 nm.

5. Conclusion

The measurements of single scattering by particles in air and scattering by particulate surfaces of different minerals and volcanic ash reveal that the single scattering NPBs can be a dominant factor in formation of NPBs of at least some particulate surfaces. Our evidence is based also on various computer simulations. In addition, the simulations demonstrate that the opposite effect to what we observe in the measurements is possible, namely that the coherent multiple scattering can generate a NPB when single particles constituting the sample do not have a NPB. The model predicts bi-modal NPBs for dark regolith-like surfaces, although in laboratory measurements we find only a slight hint of such bi-modality.

Acknowledgements

This work was supported by the TechBase Program on Chemical and Biological Defense and by the Battlefield Environment Directorate under the auspices of the U.S. Army Research Office Scientific Services Program administered by Battelle (Delivery Order 291, Contract. No. DAAD19-02-D-0001). The work of Olga Muñoz was partially supported by contracts, PNE-001/2000-C-01 and AYA2001-1177.

References

[1] Shkuratov Yu, Videen G, Kreslavsky M, Belskaya I, Kaydash V, Ovcharenko A, Omelchenko V, Opanasenko N, Zubko E. Scattering properties of planetary regoliths near opposition. In: Videen G, Yatskiv Ya, Mishchenko M, editors. Photopolarimetry in remote sensing. NATO Science Series. Netherlands: Kluwer Academic Publishers; 2004:191–208.

[2] Lyot B. Recherches sur la polarisation de la lumiere des planetes et de queldues substances terrestres. Ann Obs Meudon 1929;8:1.

[3] Shkuratov YuG. On the origin of the opposition effect and negative polarization for cosmic bodies with solid surface. Astronomicheskii Circular (Sternberg State Astron Inst, Moscow) 1985;1400:3–6.

[4] Shkuratov YuG. The diffraction mechanism of opposition effect of surface with complex structure. Kinematika i Fisika Nebesnykh Tel 1988;4:33–9.

[5] Shkuratov YuG. Interference mechanism of opposition spike and negative polarization of atmosphereless planetary bodies. Bull Am Astron Soc 1989;21 (3):989.
[6] Shkuratov YuG. A new mechanism of the negative polarization of light scattered by the surfaces of atmosphereless celestial bodies. Astronomicheskii Vestnik 1989;23:176–80.
[7] Shkuratov YuG. An interference model of the negative polarization of light scattered by atmosphereless celestial bodies. Solar System Res 1991;25:134–42.
[8] Shkuratov Yu, Muinonen K, Bowell E, Lumme K, Peltoniemi J, Kreslavsky M, Stankevich D, Tishkovets V, Opanasenko N, Melkumova L. A critical review of theoretical models for the negative polarization of light scattered by atmosphereless solar system bodies. The Earth Moon and Planets 1994;65:201–46.
[9] Muinonen K. Electromagnetic scattering by two interacting dipoles. in: Proc. 1989 URSI Electromagnetic Theory Sympos.. Sweden: Stockholm; 1989. pp. 428–30.
[10] Muinonen K. Coherent backscattering by solar system dust particles. in: Milani A, Di Martino M, Cellino A., (editors.) Asteroids, comets and meteors. Netherlands: Kluwer Academic Publishers; 1993. pp. 271–96.
[11] Mishchenko MI. The angular width of the coherent backscattering opposition effect: an application to icy outer planet satellites. Astrophys Space Sci 1992;194:327–33.
[12] Mishchenko MI, Dlugach JM. Coherent backscattering and the opposition effect for E-type asteroids. Planet Space Sci 1993;41:173–81.
[13] Mishchenko MI. Polarization effects in weak localization of light: calculation of the copolarized and depolarized backscattering enhancement factors. Phys Rev B 1991;44:12579–600.
[14] Mishchenko MI. Enhanced backscattering of polarized light from discrete random media. J Opt Soc Am A 1992;9: 978–82.
[15] Mishchenko MI, Luck J-M, Nieuwenhuizen TM. Full angular profile of the coherent polarization opposition effect. J Opt Soc Am A 2000;17:888–91.
[16] Mishchenko M, Tishkovets V, Litvinov P. Exact results of the vector theory of coherent backscattering from discrete random media: an overview. in: Videen G, Kocifa M., (editors.) Optics of cosmic dust. Dordrecht: Kluwer Academic Publishers; 2002. pp. 239–60.
[17] Videen G. The negative polarization branch and second-order ray-tracing. Appl Opt 2002;41:5115–21.
[18] Videen G. Polarization opposition effect and second-order ray-tracing: cloud of dipoles. JQSRT 2003;79–80:1103–9.
[19] Litvinov PV, Tishkovets VP, Muinonen K, Videen G. Coherent opposition effect for discrete random media: from theory to applications. in: van Tiggelen B, Skepetrov S., (editors.) Wave scattering in complex media. Dordrecht: Kluwer Academic Publishers; 2003. pp. 567–81.
[20] Tishkovets VP, Litvinov PV, Lyubchenko MV. Coherent opposition effects for semi-infinite discrete random medium in the double-scattering approximation. JQSRT 2002;72:803–11.
[21] Hapke B. Coherent backscattering and the radar characteristics of outer planet satellites. Icarus 1990;88:407–17.
[22] Hapke B. Theory of reflectance and emittance spectroscopy. Cambridge: Cambridge University Press; 1993. 450p.
[23] Shkuratov Yu, Ovcharenko A, Zubko E, Miloslavskaya O, Nelson R, Smythe W, Muinonen K, Piironen J, Rosenbush V, Helfenstein P. The opposition effect and negative polarization of structurally simulated planetary regoliths. Icarus 2002;159:396–416.
[24] Shkuratov Yu, Ovcharenko A. Experimental modeling of opposition effect and negative polarization of regolith-like surfaces. in: Videen G.Kocifaj M., (editors.) Optics of cosmic dust. NATO Science Series, London: Kluwer Academic Publishers; 2002. pp. 225–38.
[25] Rosenbush V, Avramchuk V, Rosenbush A, Mishchenko M. Polarization properties of the Galilean satellites of Jupiter: observations and preliminary analysis. Astrophys J 1997;487:402–14.
[26] Rosenbush V, Kiselev N, Avramchuk V, Mishchenko M. Photometric and polarimetric opposition phenomena exhibited by solar system bodies. in: Videen G, Kocifaj M., (editors.) Optics of cosmic dust. NATO Science Series. Netherlands: Kluwer Academic Publishers; 2002. pp. 191–224.
[27] Hapke B. Lunar surface composition inferred from optical properties. Science 1968;159 (3810):76–9.
[28] Muñoz O, Volten H, de Haan J, Vassen W, Hovenier J. Experimental determination of scattering matrices of olivine and Allende meteorite particles. Astron Astrophys 2000;360:777–88.
[29] Muñoz O, Volten H, Hovenier J. Experimental light scattering matrices relevant to cosmic dust. in: Videen G, Kocifaj M., (editors.) Optics of cosmic dust. NATO Science Series. London: Kluwer Academic Publishers; 2002. pp. 57–70.

[30] Muñoz O, Volten H, de Haan J, Vassen W, Hovenier J. Experimental determination of the phase function and degree of linear polarization of El Chichon and Pinatubo volcanic ashes. J Geophys Res 2002;107 (D13):4-1–8.
[31] Volten H, Muñoz O, Rol E, de Haan J, Vassen W, Hovenier J, Muinonen K, Nousiainen T. Scattering matrices of mineral aerosol particles at 441.6 nm and 632.8 nm. J Geophys Res 2001;106:17,375–401.
[32] Muñoz O, Volten H, de Haan JF, Vassen W, Hovenier JW. Experimental determination of scattering matrices of randomly oriented fly ash and clay particles at 442 and 633 nm. J. Geophys. Res. 2001;106:22,833–44.
[33] Hovenier J, Volten H, Muñoz O, van der Zande W, Waters L. Laboratory studies of scattering matrices for randomly oriented particles. In: Gustafson B, Kolokolova L, Videen G, editors. Potentials, problems, and perspectives. Electromagnetic and light scattering by nonspherical particles. Gainesville, FL, 2002. p. 127–30.
[34] Zubko ES, Kreslavsky MA, Shkuratov YuG. The role of scatterers compared to wavelength in formation of negative polarization of light. Solar System Res 1999;33:296–301.
[35] Zubko ES, Shkuratov YuG. Negative polarization of light scattered by cometary dust and planetary regolith: two different mechanisms. Abstract of symposium “Solar System Remote Sensing” 2002. Pittsburgh: Pitt Univ. Abstract #4002.
[36] Zubko ES, Shkuratov YuG. Mechanisms of negative polarization for planetary regolith and cometary dust. Abstr. of paper. 36th International Microsymosium on Planetology, 14–16 October. 2002, GEOKHI Moscow, abstract MS 101.
[37] Zubko E, Shkuratov Yu, Hart M, Eversole J, Videen G. Backscattering and negative polarization of agglomerate particles. Opt Lett 2003;28:1504–6.
[38] Zubko E, Ovcharenko A, Shkuratov Yu Polarimetric weak-localization effect in scattering of natural light in the region of small phase angles. Opt Spectrosc 2002;92:443–8.
[39] Shkuratov YuG, Ovcharenko AA, Stankevich DG, Korokhin VV. A study of light backscattering from planetary-regolith-type surfaces at phase angles 0.2–3.5 degrees. Sol Syst Res 1997;31:56–63.
[40] Shkuratov YuG, Kreslavsky MA, Ovcharenko AA, Stankevich DG, Zubko ES, Pieters C, Arnold G. Opposition effect from Clementine data and mechanisms of backscattering. Icarus 1999;141:132–55.
[41] Ovcharenko A, Shkuratov Yu, Nelson R. Characteristics of light scattering at small phase angles by surface consisting of spherical particles. Sol Syst Res 2001;35:291–8.
[42] Nelson R, Hapke B, Smyth W, Shkuratov Yu, Ovcharenko A, Stankevich D. The reflectance phase curves at very small phase angle: a comparative study of two goniometers. Lunar and Planet. Sci. 30th. LPI Houston. 1999; Abstract #2068.
[43] Konert M, Vanderberghe J. Comparison of laser grain analysis with pipette and sieve analysis: a solution for the underestimation of the clay fraction. Sedimentology 1997;44:532–5.
[44] Hansen JE, Travis LD. Light scattering in planetary atmospheres. Space Sci Rev 1974;16:527–610.
[45] Purcell EM, Pennypacker CR. Scattering and absorption of light by nonspherical dielectric grains. Astrophys J 1973;186: 705–14.
[46] Draine BT. The discrete-dipole approximation and its application to the interstellar graphite grains. Astrophys J 1988;333:848–72.
[47] Draine BT, Flatau PJ. Discrete-dipole approximation for scattering calculations. J Opt Soc Am A 1994;11:1491–8.
[48] Draine BT, Goodman JJ. Beyond Clausius–Mossotti: wave propagation on a polarizable point lattice and the discrete dipole approximation. Astrophys J 1993;405:685–97.
[49] Flatau P, Fuller K, Mackowski D. Scattering by two spheres in contact: comparisons between the discrete dipole approximation and modal analysis. Appl Opt 1993;32:3302–5.
[50] Lumme K, Rahola J. Light scattering by porous dust particles in the discrete-dipole approximation. Astrophys J 1994;425:653–67.
[51] Muinonen K, Videen G, Zubko E, Shkuratov Yu Coherent backscattering by discrete random media: numerical techniques. in: Videen G, Kocifaj M., (editors.) Optics of cosmic dust. NATO Science Series. London: Kluwer Academic Publishers; 2002. pp. 261–82.
[52] Videen G, Muinonen K, Lumme K. Coherence power laws and the negative polarization surge. Appl Opt 2003;42: 3647–52.
[53] Hovenier JW. Measuring scattering matrices of small particles at optical wavelengths. in: Mishchenko MI, Hovenier JW, Travis LD., (editors.) Light scattering by nonspherical particles. San Diego: Academic Press; 2000. pp. 355–65.